Biochimica et Biophysica Acta 1788 (2009) 358–370

Contents lists available at ScienceDirect

Biochimica et Biophysica Acta

journal homepage: www.elsevier.com/locate/bbamem

Environmental tobacco smoke effects on lung surfactant film organization

Patrick C. Stenger [a], Coralie Alonso [a], Joseph A. Zasadzinski [a,*], Alan J. Waring [b], Chun-Ling Jung [b], Kent E. Pinkerton [c]

[a] Department of Chemical Engineering, University of California, Santa Barbara, CA 93106-5080, USA
[b] Departments of Medicine and Pediatrics, UCLA School of Medicine, Los Angeles, CA 90095, USA
[c] Department of Anatomy, Physiology and Cell Biology, School of Veterinary Medicine, University of California, Davis, CA 95616, USA

ARTICLE INFO

Article history:
Received 7 May 2008
Received in revised form 13 November 2008
Accepted 14 November 2008
Available online 11 December 2008

Keywords:
Pulmonary surfactant
Inhibition
Inactivation
Second-hand smoke
Adsorption
Phospholipids

ABSTRACT

Adsorption of the clinical lung surfactants (LS) Curosurf or Survanta from aqueous suspension to the air–water interface progresses from multi-bilayer aggregates through multilayer films to a coexistence between multilayer and monolayer domains. Exposure to environmental tobacco smoke (ETS) alters this progression as shown by Langmuir isotherms, fluorescence microscopy and atomic force microscopy (AFM). After 12 h of LS exposure to ETS, AFM images of Langmuir–Blodgett deposited films show that ETS reduces the amount of material near the interface and alters how surfactant is removed from the interface during compression. For Curosurf, ETS prevents refining of the film composition during cycling; this leads to higher minimum surface tensions. ETS also changes the morphology of the Curosurf film by reducing the size of condensed phase domains from 8–12 μm to ~2 μm, suggesting a decrease in the line tension between the domains. The minimum surface tension and morphology of the Survanta film are less impacted by ETS exposure, although the amount of material associated with the film is reduced in a similar way to Curosurf. Fluorescence and mass spectra of Survanta dispersions containing native bovine SP-B treated with ETS indicate the oxidative degradation of protein aromatic amino acid residue side chains. Native bovine SP-C isolated from ETS exposed Survanta had changes in molecular mass consistent with deacylation of the lipoprotein. Fourier Transform Infrared Spectroscopy (FTIR) characterization of the hydrophobic proteins from ETS treated Survanta dispersions show significant changes in the conformation of SP-B and SP-C that correlate with the altered surface activity and morphology of the lipid–protein film.

1. Introduction

Environmental tobacco smoke (ETS) is the smoke inhaled by bystanders (also called passive smokers) and is a combination of smoke emitted from the smoldering cigarette (sidestream smoke) and smoke exhaled by the smoker (mainstream smoke) [1,2]. ETS is qualitatively similar in composition to mainstream smoke and contains the same carcinogens, toxic compounds and oxidizers, albeit at lower concentrations than those inhaled by smokers [1]. Exposure to ETS has been causally linked to lung cancer [1,3–6] and has some association with asthma in never-smoking adults [1,5]. In children, ETS exposure has been linked to lower respiratory tract infections, asthma induction and exacerbation, and chronic respiratory symptoms such as wheezing and coughing [1,5,7,8]. However, recognizing the negative effects of ETS in large populations does not explain the origin of these effects in individuals, or the effects at the molecular scale. This limits the interventions to control or reverse ETS exposure.

Regardless of other mechanisms of action, ETS must interact with the epithelial lining fluid (ELF), the fluid layer which lines the lungs and contains antioxidants and lung surfactant (LS) [9]. The oxidants in ETS can react to form even more reactive agents or degrade or inactivate the components of the ELF. Since the ELF is thinner in the lower airways and alveoli and contains a lower concentration of antioxidants than the upper airways, damage from inhaled oxidants such as ETS likely occurs in the alveoli and lower airways with LS being especially vulnerable [9].

LS is a mixture of lipids and four lung specific proteins (SP-A, B, C, and D) that lines the ELF in the interior of the lung alveoli (and to a lesser extent in the bronchi and bronchioles) and acts to lower interfacial tension [10,11]. A low surface tension in the lungs, especially on expiration, leads to a negligible work of breathing and uniform lung inflation [10]. The absence of LS due to prematurity causes neonatal Respiratory Distress Syndrome (NRDS), which is characterized by atelectasis (collapse of the alveoli) and reduced gas exchange [10–13] and an increased effort needed to breathe. Treating NRDS with currently available replacement clinical surfactants has significantly reduced neonatal mortality in developed countries [10–12,14,15].

* Corresponding author. Tel.: +1 805 893 4769; fax: +1 805 893 4731.
E-mail address: gorilla@engineering.ucsb.edu (J.A. Zasadzinski).

0005-2736/$ – see front matter © 2008 Elsevier B.V. All rights reserved.
doi:10.1016/j.bbamem.2008.11.021

Survanta is one such replacement surfactant used to treat NRDS; Survanta is an organic extract of minced bovine lung that is supplemented with dipalmitoylphosphatidylcholine (DPPC), palmitic acid, and triacylglycerol. Survanta contains 80–90 wt.% phosphatidylcholine, of which, ~70 wt.% is saturated DPPC [16]. About 7 wt.% of the phospholipids are negatively charged. Survanta contains sub-physiological levels of the amphiphilic lung surfactant specific protein SP-B (0.04–0.13%; g/g lipid) and closer to physiological levels of hydrophobic lung surfactant specific protein SP-C (0.4–0.9%; g/g lipid) [16,17]. Curosurf is an extract of whole minced porcine lung tissue purified by column chromatography that contains 70–75 wt.% phosphatidylcholine, of which, ~37 wt.% is DPPC and ~26 wt.% is unsaturated lipids [16]. It contains 0.3 % (g/g lipid) SP-B, 0.7 % (g/g lipid) SP-C and 5 wt.% negatively charged phospholipids [16,17]. In both preparations, cholesterol and the hydrophilic LS proteins SP-A and SP-D are removed. In this work, we use Survanta and Curosurf as compositionally well-defined model surfactants to determine the effects of ETS on lung surfactant film organization and structure and how these effects depend on changes in surfactant composition.

The common features of native and replacement lung surfactants suggest that a minimum, but so far, not universally accepted set of lipid and protein components is necessary for proper lung surfactant function [10,12,14–16,18–28]. SP-B forms multilayer structures in conjunction with anionic unsaturated lipids [23] as well as monolayer folds at low surface tension [29]. Model mixtures containing SP-B [30] and unsaturated anionic lipids show a characteristic plateau in the isotherm similar to Survanta and Curosurf [23,24]. SP-C [31] promotes the formation of multilayer domains in simple lipid mixtures [21,22,24,32,33] and regulates the surface viscosity of surfactant films [22,33]. A balance between saturated lipids that form semi-crystalline solid phases, and unsaturated lipids that form disordered, liquid-like phases under physiological conditions is also likely to be essential to proper surfactant adsorption and low surface tensions [16,21,22,25,26,33–36]. The synergistic nature of these lipid–protein and lipid–lipid interactions suggests that any degradation of surfactant proteins due to ETS exposure may result in deleterious changes in surfactant performance [9,28,37–39]. Absolute analysis of these effects of ETS is complicated by the lack of a generally accepted lipid and protein formulation for either native or replacement lung surfactants; for example, the ratio of saturated to unsaturated lipids varies widely between clinical surfactants [16], as does the fraction of cholesterol [14–16,28]. There are also substantial variations in the composition of native lung surfactants measured by different methods, as well as variations between species [10,12,30,40,41].

ETS contains oxidants, free radicals and other components that can chemically and physically degrade LS components [1,2,9,37,39]. Oxidation of lung surfactant lipids and proteins *in vivo* results in impaired surfactant function and altered surfactant composition, though the response is oxidizer and model dependant [9]. *In vitro*, oxidation by Fenton regents or hypochlorous acid of surfactant formulations yields a decrease in unsaturated lipids (phosphatidylglycerols, phosphatidylcholines) and a corresponding increase in lysolipids (lysophosphatidylglycerols, lysophosphatidylcholines) [39]. Oxidation of SP-B leads to a decreased recognition by the anti-SP-B antibody and can induce conversion of the tryptophan-9 (Trp9) of SP-B to hydroxyTrp, N-formylkynurenine and kynurenine [38]. SP-C oxidation leads to lower levels of palmitoylation [31], which can lead to loss of the alpha-helical structure [42] as well as decreased surfactant film stability and compressibility [21,32,42,43]. Generally, oxidized phospholipid or phospholipid/protein formulations result in a larger minimum surface tension at the same amount of compression as the control [37,39], with protein oxidation more deleterious to surface activity than lipid oxidation. Another study of phospholipid/protein formulations exposed to reactive oxygen species found that the hydroxyl radical had broad inhibitory effects on surface activity while superoxide anion altered some film properties but not the minimum surface tension [44].

Previous work studying the impact of ETS on LS has focused on compositional changes, although preliminary work has been done on LS film morphology and surface activity [37,45–51]. Exposure to cigarette smoke has been shown to reduce the amount of SP-B in bronchoalveolar lavage in rats [50] and the amount of SP-A and SP-D in humans [46]. Maternal exposure to nicotine reduced the amount of lung surfactant lipids present in newborn rats and altered the expression of the surfactant proteins [45]. When exposed to cigarette smoke *in vitro*, the number of type II alveolar cells producing lung surfactant decreased [51]. However, the amount of surfactant produced per type II cell increased leading to no change in the total surfactant production. Bronchoalveolar lavage of rats exposed to cigarette smoke shows a significant decrease in saturated phosphatidylcholines while total phospholipid content was unchanged yielding isotherms with decreased surface activity [48]. However, a subsequent study with environmental cigarette smoke showed little difference in lipid and protein content or surface activity in smoke exposed rats or controls [49].

To determine the changes in LS organization and self-assembly that occur after exposure to ETS, we measure surface pressure, Π, ($\Pi = \gamma_w - \gamma$; γ_w is the surface tension of a clean water interface, 72 mN/m, and γ the measured surface tension) vs. area isotherms [37] with a Langmuir trough as an *in vitro* model of the epithelial lining fluid. Both Survanta and Curosurf exposed to ETS for 12–24 h (roughly corresponding to the turnover of lung surfactant in the alveolus [12]) are deposited from aqueous suspension so that the surfactant adsorbs to the air–water interface from the subphase. Adsorption from the subphase to the air–liquid interface is more physiologically relevant than spreading from an organic solvent and allows us to study the effects of ETS exposure on the adsorption and self-assembly of the films. This spreading approach also captures *in vitro* that LS is not just a simple monolayer but also has a surface associated "reservoir" adjacent to the air–water interface that impacts LS performance [33,52–55]. Chemical variations in the LS proteins SP-B and SP-C in Survanta are characterized using FTIR, fluorescence emission spectroscopy, and mass spectroscopy after isolation of the hydrophobic surfactant proteins by column chromatography, gel electrophoresis and freeze-drying.

ETS exposure reduces the amount of material in the surface associated reservoir, suggesting changes in the mechanisms of surfactant adsorption and desorption for both Survanta and Curosurf. Curosurf, which contains a higher fraction of unsaturated lipids and proteins (especially SP-B), is more adversely affected; isotherms show that ETS prevents refining of the film composition during cycling leading to reduced surface activity. Fluorescence microscopy images reveal that ETS reduces the size of condensed phase domains from 8–12 μm to ~2 μm, suggesting an alteration in the line tension. In contrast, the minimum surface tension and morphology of the Survanta film are less impacted by ETS exposure, perhaps due to the higher content of saturated lipids in Survanta. The secondary structure of SP-B in Survanta films exposed to ETS changes in ways that are consistent with a less functional conformation of the protein. Fluorescence emission spectroscopy shows the presence of N-formylkynurenine and kynurenine, oxidation products of tryptophan in SP-B [38] that are confirmed by mass spectra. Conformational analysis of SP-C from ETS-exposed Survanta indicates a change in the protein secondary structure that correlates with deacylated SP-C, which was confirmed by mass spectroscopy [56]. These changes in SP-C limit the formation and stability of the surface-associated LS reservoir [21,32,33,57]. ETS, like other oxidizers [9,38,39], degrades lung surfactant performance *in vitro*, likely through chemical degradation of the lung specific proteins SP-B and SP-C and unsaturated lipids.

2. Experimental

2.1. Sample preparation

Curosurf was purchased from Dey Laboratories (Napa, CA) and Survanta (Abbott Laboratories, Columbus, Ohio) was excess product used in the UCSF nursery. ETS water was generated by a smoke exposure system located at the UC Davis Institute of Toxicology and Environmental Health [2]. 1RF4 reference cigarettes were burned at 22 °C and 49% relative humidity in a temperature and humidity controlled smoking machine. An 89% mainstream-11% side-stream smoke mixture was collected and mixed with a fresh air stream for a mean residence time of 2 min. The concentrations of carbon monoxide, nicotine and total suspended particulates (TSP) in the smoke mixture were 241 ± 6 ppm, 12.0 mg/m^3, and 77 ± 9 mg/m^3 respectively. All water used in experiments was obtained from a Millipore Gradient System (Billerica, MA) and had a resistivity of 18.2 MΩ/cm. A fixed volume of Millipore water was exposed to the smoke mixtures for 6 h and then refrigerated until used in experiments. The Curosurf and Survanta stock solutions were diluted to 2 mg/ml suspensions with Millipore water and/or ETS-exposed water. Survanta forms multimicron, irregularly shaped bilayer aggregates in buffered saline solutions while Curosurf forms micron to submicron spherical multilamellar vesicles [17], consistent with the significantly larger fraction of saturated lipids in Survanta. Samples in ETS-exposed water were incubated 12–24 h under refrigeration before sample characterization as noted. Concentrations of the spreading solutions are listed as the equivalent TSP concentration, 0–77 mg/m^3; this range was similar to previous investigations of the effects of ETS [2,37].

To analyze the chemical effects of ETS on SP-B and SP-C, Survanta suspended for 24 h in ETS water was carefully collected from the air–water interface of a Langmuir trough and extracted into chloroform: methanol 2:1 [58] and the extract partitioned overnight. The extract was then concentrated by flash evaporation. SP-B and SP-C were isolated from this extract in a liquid chromatography column packed with Silica C8 (J.T. Baker, Phillipsburg, NJ) pre-equilibrated with 7:1:0.4 (v:v) MeOH:$CHCL_3$:H_2O+0.1% trifluoroacetic acid (TFA) as an ion pairing agent. The sample was then chromatographed with the same aqueous-organic solvent mixture to separate SP-B, SP-C and surfactant lipids [59]. Protein samples were then solubilized in hexafluoroisopropanol:10 mM HCl (v:v, 1:1) and twice freeze-dried to remove acetate counterions that would interfere with infrared analysis.

3. Methods

Isotherms were recorded at 25 °C (no significant changes were seen from 23–37 °C [33,37] using a custom stainless steel ribbon trough (Nima, Coventry, England) equipped with a Wilhelmy plate to measure surface pressure. The trough had a surface area of 130 cm^2, a subphase volume of 150 mL, and a typical compression/expansion cycle took 15 min. The ribbon trough was used to minimize losses due to leakage as the steel ribbon provided a continuous barrier to the surfactant. The stated concentrations of Survanta and Curosurf dispersions were deposited dropwise onto the saline buffer subphase (150 mM NaCl, 2 mM $CaCl_2$, and 0.2 mM $NaHCO_3$, pH=7) of the Langmuir trough at the stated total surfactant concentrations and allowed to equilibrate 20 min before beginning cycling. Surfactant deposited in this fashion adsorbs from the subphase to the interface as multilayer aggregates that convert to a monolayer on contact with the air–water interface [33,60,61].

A Nikon Optiphot optical microscope (Nikon, Tokyo, Japan) was positioned above the trough with a 50× extra-long working distance objective (Nikon) designed for fluorescent light. Full-length movies and individual frames were recorded directly to computer (Moviestar, Mountain View, CA). Contrast in the images was due to segregation of 1 mol% fluorescent lipid Texas Red-DHPE (Invitrogen, Eugene, OR) between the liquid expanded phase, which appears light gray in images, and the condensed phase, which appears black in the films [62]. Bright white areas indicate thicknesses much greater than a monolayer, which are usually associated with multilayered surfactant aggregates contacting the interface or folded or collapsed regions of the film [29,63].

Samples for AFM imaging were prepared using a vertical Langmuir–Blodgett deposition [64,65]. The substrate, held by tweezers, was put in the subphase perpendicular to the surface. 100 μL of Survanta or Curosurf aqueous suspension, diluted to 2 mg/mL (200 μg surfactant) by Millipore or ETS water, was deposited onto the subphase dropwise until the surface pressure was ~15 mN/m. The barriers were compressed to the correct surface pressure and then the substrate was slowly pulled through the interface while the surface pressure was held constant. Mica substrates were cleaved with ordinary adhesive tape immediately before use. The film covered mica surfaces were transferred to a modified Nanoscope III AFM (Digital Instruments, Santa Barbara, CA) for imaging under ambient conditions. AFM imaging was done with a 150 μm × 150 μm (J) scanner in contact mode in air at ambient temperature. Silicon nitride tips with a spring constant of 0.12 N/m were used. Excessive force on the sample was a concern during imaging, so samples were checked often for deformation by imaging a smaller region (10×10 μm), then imaging at 50×50 μm to check if the smaller region was damaged. Under the deposition and imaging conditions used here, the hydrophobic or air-side of the film is facing outward from the mica and is the surface being imaged [64,65].

Infrared spectra were recorded at 25 °C using a Bruker Vector 22™ FTIR spectrometer with a DTGS detector, averaged over 256 scans at a gain of 4 and a resolution of 2 cm^{-1}. Protein self-films were prepared by air-drying hexaflouroispropanol (HFIP) solutions of the material onto a 50×20×2 mm, 45° ATR crystal fitted for the Bruker (Pike Technologies) spectrometer [66,67]. The sample was then overlaid with HFIP to insure saturation of the peptide with the organic solvent before measuring the IR spectrum. The relative proportions of α-helix, β-turn, β-sheet, and disordered conformations of the resulting IR spectra were determined by Fourier self-deconvolution for band narrowing and area calculations of component peaks of the FTIR spectra using curve-fitting software supplied by Galactic Software (GRAMS/32, version 5; Galactic Industries Corp., Salem, NH). The frequency limits for the different structures were: α-helix (1662–1645 cm^{-1}), β-sheet (1637–1613 and 1710–1682 cm^{-1}), β-turns (1682–1662 cm^{-1}), and disordered or random (1650–1637 cm^{-1}) [68].

Steady-state fluorescence emission spectra of the aromatic residues in the SP-B protein were made at 25 °C, in reagent ethanol, with a Cary Eclipse Fluorescence spectrophotometer at excitation wavelengths of 275, 325, or 365 nm and with slit widths of 0.5 nm for excitation and emission monochrometers and a photomultiplier tube setting of 800 V. Fifty μl of the surfactant protein sample were added to 1 ml of reagent alcohol in a quartz sample cuvette and an emission spectrum at the relevant wavelength was obtained to detect the presence of tryptophan (Trp), tyrosine (Tyr), N-formylkynurenine and kynurenine.

Changes in the mass of hydrophobic surfactant proteins from ETS exposed samples of Survanta were determined by MALDI-TOF mass spectrometry. SP-B and SP-C proteins were isolated by isocratic elution using Octyl (C8) preparative liquid chromatography as described above. The eluted protein fractions were then identified by SDS-PAGE gel electrophoresis (10–20% Tricine Gel, Invitrogen, Carlsbad, CA). Bands corresponding to the approximate molecular weights of SP-B and SP-C were cut out from the gel, destained and eluted from the gel using 80% acetonitrile–water. The eluted protein fractions were then mixed with α-cyano-4-hydroxycinnamic acid – 3,5-dimethoxy-4-hydroxy-cinnamic acid matrix (Sigma, Saint Louis, MO) and spotted on an Applied Biosystems V700666 MALDI-TOF plate

prior to mass determination. Protein samples were measured using an Applied Biosystems Voyager-DE STR MALDI-TOF mass spectrometer (Applied Biosystems, Foster City, CA) in the linear mode with delayed extraction and negative polarity.

4. Results

4.1. Isotherms

Fig. 1 shows typical compression–expansion isotherms for pristine and ETS-exposed (TSP=77 mg/m^3) Curosurf (300 μg) and Survanta (200 μg) on a saline buffer subphase. The amount of surfactant was chosen to have an initial surface pressure of 15–20 mN/m after 20 min of adsorption. The compression isotherms had a characteristic plateau at $\Pi \sim 40$ mN/m followed by a rapid surface pressure increase leading to a second plateau, also known as the collapse plateau, at $\Pi \sim 65$ mN/m [12,33,54,55]. The length of the plateau at ~40 mN/m is more pronounced for the first cycle of Curosurf and decreases with subsequent cycles [12,33]. The hysteresis between compression and expansion cycles is typical of clinical lung surfactant isotherms [12] as well as most preparations of native surfactant [14,69]. Compressing the lung surfactant film leads to collapse at a surface pressure much in excess of the equilibrium spreading pressures of the surfactants, which are ~40 mN/m for Curosurf and Survanta [70]. Expanding the interface after monolayer collapse leads to a rapid drop in surface pressure, which is maintained until compression is resumed. This drop in surface pressure is well below the equilibrium spreading pressure of the surfactant. Increasing cycles (arrow) show the length of the collapse plateau ($\Pi \sim 66$) increases to about 15% of the total trough area, reaching a steady state after four cycles. At the same time, the length of the first plateau, associated with unsaturated lipids, at ~40 mN/m decreases [10,12,29,32, 33].

The isotherm of ETS-exposed Curosurf in Fig. 1b shows a similar initial surface pressure from surfactant adsorption of $\Pi \sim 15$ mN/m. However, the collapse plateau at $\Pi \sim 66$ mN/m has almost vanished, comprising only 2% of the total trough area even after the isotherm reaches a steady state. The length of the characteristic shoulder at ~40 mN/m decreases with cycling in the ETS-exposed Curosurf, but this is due to the steady movement of the break in the isotherm to lower trough areas. Hence, there is no corresponding increase in the length of the collapse plateau as seen in the unexposed Curosurf (Fig. 1a). In Fig. 1a, the break in the isotherm at ~40 mN/m occurs at a trough area of ~60% on each cycle, and the increase to the collapse pressure occurs at larger trough areas with each cycle. The surface pressure at full expansion decreases with the number of cycles for the ETS exposed Curosurf. It requires about a 4:1 compression ratio to reach low surface tensions after Curosurf has been exposed to ETS, compared to the 2:1 compression ratio for the pristine Curosurf for identical amounts of deposited Curosurf. This suggests that ETS exposure decreases the ability of Curosurf to adsorb to the air–water interface from the subphase [60].

Fig. 1c and d show four cycles of pristine Survanta and ETS-exposed Survanta isotherms starting from similar initial surface pressures of $\Pi \sim 20$ mN/m. In Survanta (Fig. 1c), increasing cycles (arrow) show the length of the collapse plateau reaches about 35% of the total trough area and there is a modest decrease in the length of the characteristic shoulder at 40 mN/m. Compared to the Curosurf film, the changes in the isotherm with number of cycles are more subtle in Survanta. ETS-exposed Survanta also shows a collapse plateau, which extends over about 35% of the total trough area, similar to Survanta on a pristine interface, and also apparently undergoes less alteration after initial adsorption.

4.2. Fluorescence microscopy

Fig. 2 shows fluorescence images of Curosurf and ETS (TSP=77 mg/m^3) exposed Curosurf at 25 °C on the second cycle. Discrete black domains coexist in a continuous medium gray background, similar to model lung surfactant lipid–protein mixtures and other commercial lung surfactants [13, 60, 61]. The dark domains are condensed phases

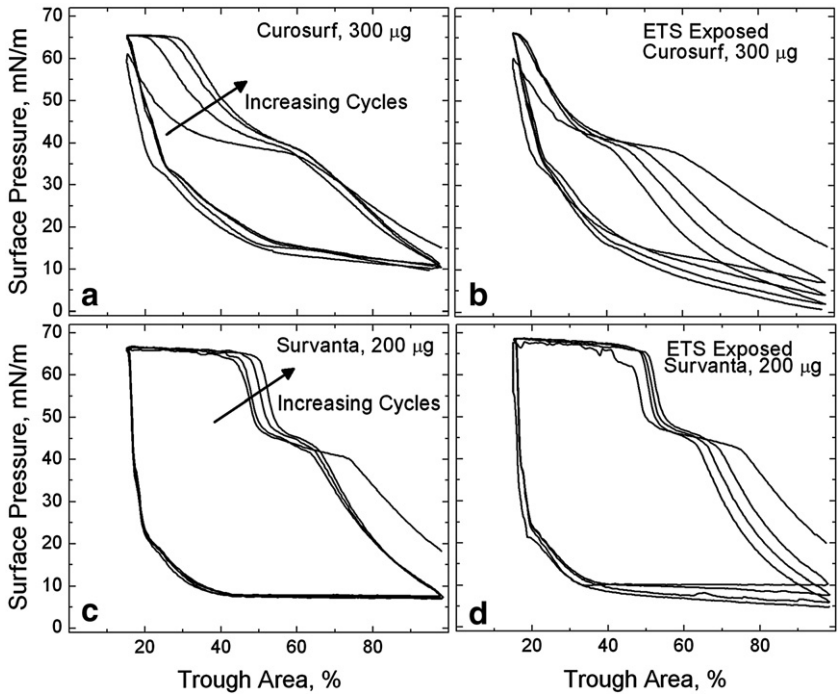

Fig. 1. Cyclic isotherms of pristine and ETS-exposed (TSP=77 mg/m^3) commercial replacement lung surfactants on a saline buffer subphase. On compression, the isotherms exhibit a characteristic shoulder at $\Pi \sim 40$ mN/m and a collapse plateau at $\Pi_{max} \sim 66$ mN/m. (a) 300 μg pristine Curosurf. The fourth cycle collapse plateau here accounts for 15% of the total trough area. (b) 300 μg ETS-exposed Curosurf. In contrast to (a), the fourth cycle collapse plateau only accounts for 2% of the total trough area. (c) 200 μg pristine Survanta (d) 200 μg ETS-exposed Survanta. In both (c) and (d), the fourth cycle collapse plateau accounts for 34% of the total trough area. Arrows indicate increasing number of compression/expansion cycles.

(typically semi-crystalline areas enriched in saturated lipids [20,25,26,35]) that exclude the bulky fluorophore-labeled Texas Red-DHPE, which cannot pack into a crystalline lattice [62]. The black domains are circular to elliptical in shape and their diameters range from the resolution limit of the optics (~1 μm) to ~12 μm. Coexistence between condensed and liquid expanded phases is typical for both Curosurf and Survanta monolayers and occurs at all surface pressures from zero to collapse [22,26,29,33]. Larger condensed domains (8–12 μm) occur more frequently in the Curosurf images (Fig. 2a,c,e,g,i) at any given surface pressure compared to ETS-exposed Curosurf (Fig. 2b,d,f,h,j). ETS suppresses the formation of the larger domains yielding smaller, more monodisperse condensed phase domains. In the ETS-exposed Curosurf at Π=20 mN/m (Fig. 2b), the average domain is approximately 2 μm, which is only slightly larger than the resolution limit of the optics. At higher surface pressures (Fig. 2d, 2f), it is unclear whether the dark domains are simply smaller than the resolution of the optics or whether they disappear entirely, leaving only a small population of 5–8 μm dark domains in the ETS-exposed Curosurf images.

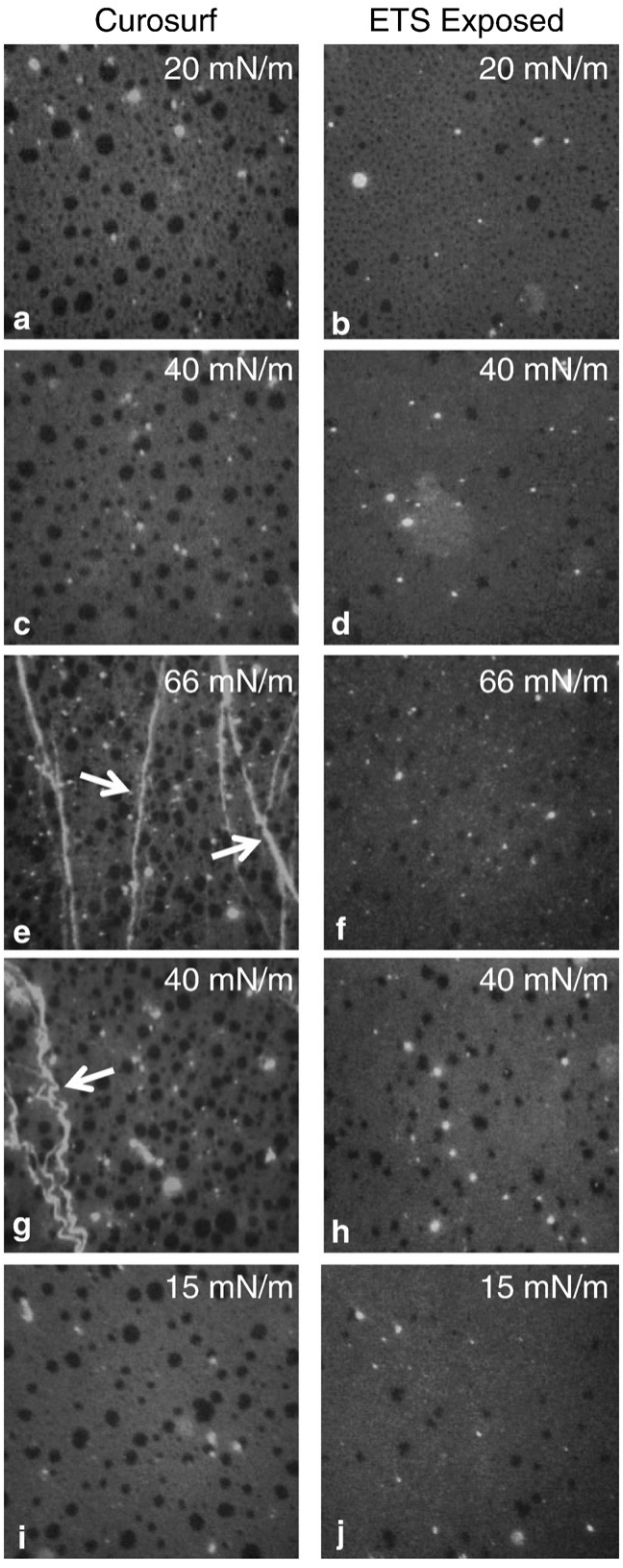

A small number of circular white domains, which indicate an accumulation of dye, and hence, surfactant, in the subphase attached to the monolayer [60], are also present at all surface pressures. These bright patches are thicker than a monolayer and are parts of the surface-associated reservoir of surfactant. Through-focus series show that the patches are on the subphase side of the monolayer. The concentration of these bright domains increases with higher surface pressure in both Curosurf and ETS-exposed Curosurf.

At the collapse pressure, Π=66 mN/m (Fig. 2e), cracks and folds (arrows) are present in Curosurf. As suggested by a recent theoretical model, the collapse folds in Fig. 2e are roughly parallel to each other and are perpendicular to the compression direction [63]. Several smaller folds have coalesced into the brighter white, larger folds at the arrows, also as suggested by this theory [63]. The monolayer collapse determines the maximum surface pressure (minimum surface tension) that can be achieved by the film [12,18,29,63,71]. During collapse, material is forced from the monolayer into the surfactant surface-associated reservoir [12,29,32,33]. These cracks and folds are absent from the ETS-exposed Curosurf images (Fig. 2f), likely because the compression needed to reach the collapse pressure caused a much shorter collapse plateau (See Fig. 1b). According to the theory by Pocivavsek et al. [63], folds grow and coalesce on continued compression after the initial monolayer collapse; for the ETS-exposed Curosurf, monolayer collapse was not reached until the maximum compression possible in our trough (Fig. 1b). Upon expansion, the folds (arrows) in the Curosurf images (Fig. 2g) appear to buckle and undulate along their length. The folds only relax back into the monolayer when the surface pressure drops to Π=15 mN/m (Fig. 2i), consistent with the hysteresis in the isotherm, but well below the equilibrium spreading pressure of 40 mN/m. During the expansion (Fig. 2g–j), the large, black, solid phase domains are more abundant in the Curosurf images than ETS-exposed Curosurf, consistent with the retention of the saturated lipids in the film on cycling.

Fig. 3 shows fluorescence images of Survanta and ETS-exposed Survanta at 25 °C on the second cycle. In contrast to Curosurf, phase separation between the mottled bright and dark regions in Survanta is more fractal in appearance and the individual domains are smaller. Survanta has a larger percentage of saturated lipids than Curosurf [16] and a significantly larger fraction of black, condensed phase is present at all surface pressures. However, there is some fraction of lighter gray, liquid expanded phase that remains up to the collapse pressure. At Π=20 mN/m and Π=40 mN/m (Fig. 3a–d), the images show the black condensed phase forms a continuous network surrounding the lighter liquid expanded phase; the opposite of what happens for Curosurf

Fig. 2. Fluorescence images of 300 mg pristine Curosurf and ETS-exposed (TSP=77 mg/m^3) Curosurf doped with 1% mol Texas Red-DHPE. Images are 171 μm×171 μm and were acquired on the second cycle. Discrete circular condensed domains (dark) coexist with a continuous liquid expanded phase (light gray). (a) Curosurf and (b) ETS-exposed Curosurf on a saline buffered subphase at Π=20 mN/m during compression. (c) Curosurf and (d) ETS-exposed Curosurf at Π=40 mN/m during compression. (e) Curosurf and (f) ETS-exposed Curosurf at the collapse plateau, Π=66 mN/m during compression. Arrows indicate cracks and folds in the monolayer due to collapse which are only seen in the Curosurf film. (g) Curosurf and (h) ETS-exposed Curosurf at Π=40 mN/m during expansion. (i) Curosurf and (j) ETS-exposed Curosurf at Π=15 mN/m during expansion. Generally, ETS exposure reduces the concentration of large condensed domains (8–12 μm) in favor of smaller ones (~2 μm).

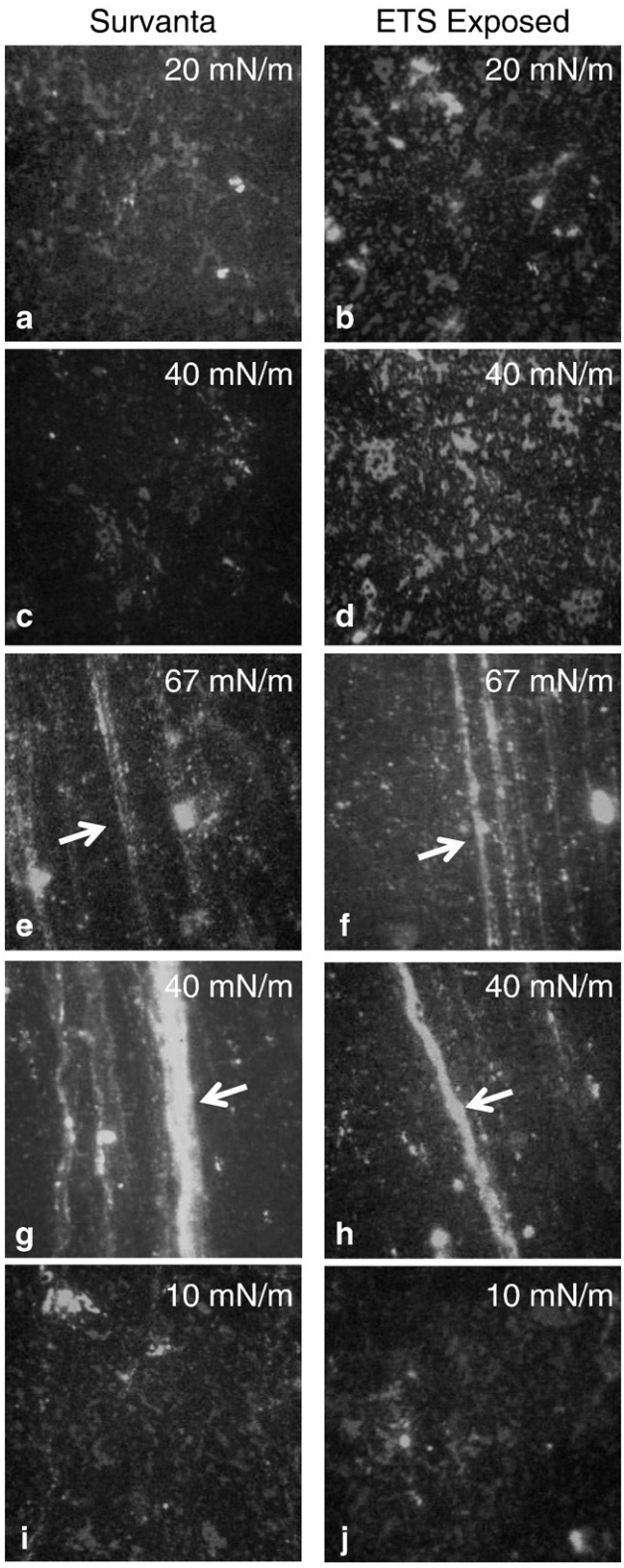

Fig. 3. Fluorescence images of 200 μg pristine Survanta and ETS-exposed (TSP = 77 mg/m^3) Survanta doped with 1% mol Texas Red-DHPE. Images are 171 μm × 171 μm and were acquired on the second cycle. The darker condensed phase forms a continuous network surrounding the lighter liquid expanded phase. (a) Survanta and (b) ETS-exposed Survanta a saline buffered subphase at Π = 20 mN/m during compression. (c) Survanta and (d) ETS-exposed Survanta at Π = 40 mN/m during compression. (e) Survanta and (f) ETS-exposed Survanta at the collapse plateau, Π = 67 mN/m, during compression. Arrows indicate cracks and folds in the monolayer due to collapse. (g) Survanta and (h) ETS-exposed Survanta at Π = 40 mN/m during expansion. (i) Survanta and (j) ETS-exposed Survanta at Π = 10 mN/m during expansion. ETS exposure has less effect on the morphology of the Survanta film than on Curosurf films.

(Fig. 2). The ETS-exposed Survanta (Fig. 3b, d) contains a greater fraction of the lighter gray, liquid expanded phase (Fig. 3a, c) although the size of the liquid expanded domains are similar. At the collapse pressure, Π = 67 (Fig. 3e, f), cracks and folds (arrows) are present in both the Survanta and ETS-exposed Survanta, consistent with the long collapse plateaus shown in the isotherms (Fig. 1c, d). These cracks and folds remain connected to the interfacial film and provide a storehouse for surfactant removed from the interface during film collapse. Upon expansion, the cracks and folds (arrows) in both samples (Fig. 2g–j) reincorporate into the monolayer only after it achieves a surface pressure of Π = 10, which, as observed for Curosurf, is the likely cause of the hysteresis in the isotherm (Fig. 1c, d). During expansion, both samples display similar mottled bright and dark texture.

ETS exposure has a smaller effect on the morphology or mechanical properties of the Survanta film compared to Curosurf. Previous work has shown that a high collapse pressure requires a threshold fraction of around 70% of the solid or LC phase [72]. The saturated lipid fraction of Survanta, even after ETS exposure, is likely high enough to provide this necessary threshold fraction of LC phase and the collapse pressure is not greatly affected by ETS exposure. However, the lower fraction of saturated lipids in Curosurf [16] may not be sufficient to achieve the threshold fraction of LC phase after ETS-exposure as film refinement appears to be compromised. In addition, Survanta has minimal levels of SP-B, so the degradation in function that likely accompanies oxidation of this protein will have a small effect.

4.3. Atomic force microscopy images

To obtain higher-resolution information regarding the interfacial films and a quantitative estimation of the domain sizes and film thickness, pristine and ETS-exposed films of Curosurf and Survanta were imaged by AFM after Langmuir–Blodgett deposition at various surface pressures [32,54,55,64,65,73]. During the transfer, material located near the air–water interface can be trapped between the mica substrate and the monolayer. Therefore, AFM can reveal the three-dimensional structure of the surface associated reservoir [53], in addition to the structure of the monolayer [22,33]. Although this complicates interpretation, AFM is the only tool that can map the three-dimensional film morphology, as many of the features seen in AFM are below the resolution of optical imaging techniques.

In general, films spread from an aqueous suspension are not a simple monolayer [33,54,55] and are quite different than AFM images of lipid or lipid/protein films spread from solvent [21,24,32,64,74]. Not all of the surfactant added to the trough necessarily adsorbs to the interface; the amount of material spread is ~15 times that necessary to form a single monolayer capable of reaching the collapse plateau upon trough compression. While some of this material never reaches the interface, surfactant films spread from aqueous suspension can have coexisting monolayer and multilayer domains [33,54,55], along with multibilayer aggregates attached to the interface [60]. Quantitative Brewster angle microscopy has also shown 12-nm-thick films adsorbing at the air–water interface from lavage fluids deposited in the subphase [75].

Representative AFM images of Curosurf and ETS-exposed Curosurf at medium (Π = 40 mN/m) and high (Π = 60 mN/m) surface pressures of the second compression isotherm are shown in Fig. 4. At 40 mN/m, low-resolution images (50 μm × 50 μm) of Curosurf (Fig. 4a) show a bright, yellow network with discrete, dark brown circular and elliptical domains similar in general appearance to the fluorescence images in the Fig. 2. In AFM images, bright means higher or thicker, and dark means thinner, as is quantified in the height traces in the third column. From the correspondence between the fluorescence and AFM images, the bright, continuous phase in FM and AFM images is the liquid expanded phase (lighter gray in Fig. 2), whereas the discrete dark domains in both FM and AFM images are condensed phase

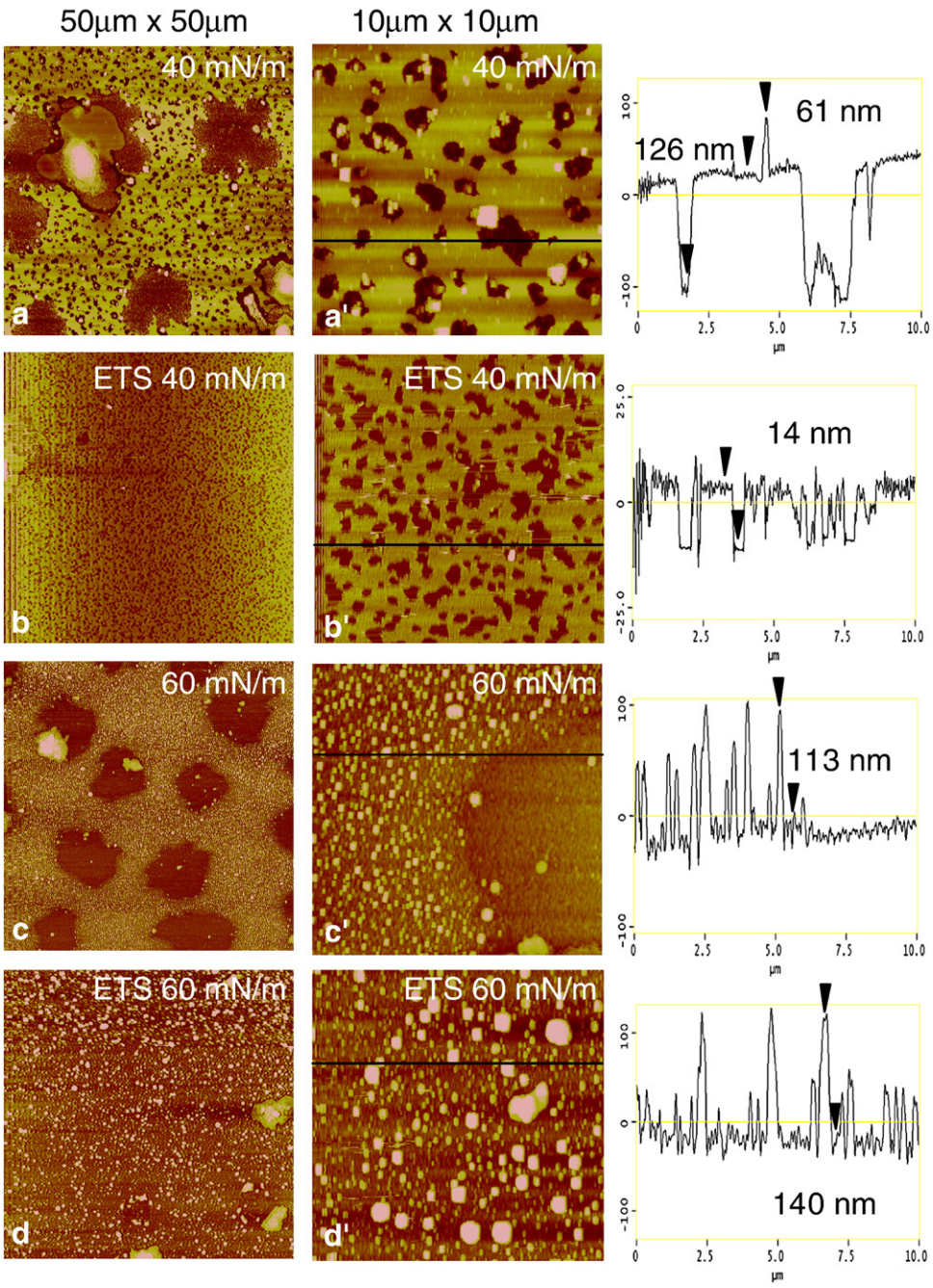

Fig. 4. Atomic force microscopy images of pristine Curosurf and ETS-exposed Curosurf transferred onto mica substrates by conventional Langmuir–Blodgett deposition. The low resolution images (left column) are 50×50 μm, and the high resolution images (right column) are 10×10 μm sections taken from the low-resolution images. The height trace in the third column corresponds to the black line on each high-resolution image. The brightness in the image increases with the height relative to the mica substrate. Images at 40 mN/m of Curosurf at (a) low and (a') high resolution and ETS-exposed Curosurf at (b) low and (b') high resolution. Discrete dark brown circular domains up to 10–15 μm wide in Curosurf (a,a') and 0.2–1 μm wide ETS-exposed Curosurf (b,b') exist in a bright yellow network. The height traces indicate a greater thickness of the bright yellow liquid expanded phase in Curosurf (~126 nm) vs. ETS-exposed Curosurf (~14 nm) indicates a larger surface associated "reservoir" which is trapped underneath the monolayer during LB deposition. Images at 60 mN/m of Curosurf at (c) low and (c') high resolution and ETS-exposed Curosurf at (d) low and (d') high resolution. Both Curosurf (c) and ETS-exposed Curosurf (d) show a non-uniform liquid expanded phase with discrete raised domains (0.3–1.3 μm wide and ~110–140 nm high) where material that has been removed from the interface is held in the surface associated reservoir. The linescans indicate a greater concentration of raised domains in Curosurf (c') demonstrating that ETS exposure (d') alters the ways that material is removed from the interface.

[33,62]. The liquid expanded (LE) phase in both AFM and FM images is continuous, and the height trace of Fig. 4a' shows that the LE phase is much thicker than the condensed domains, suggesting that the surface associated reservoir is predominantly associated with the liquid expanded phase. Much of the SP-B and SP-C is located in the liquid expanded phase, and hence associated with the unsaturated and anionic lipids [21,23,24,32]. If the proteins are involved in adsorption or stabilization of multilayer reservoirs, it is reasonable for the liquid expanded phase to be the most likely location for adsorption and desorption (squeeze-out) from the film [21,24,32].

While the majority of the dark domains in the Curosurf at 40 mN/m images (Fig. 4a,a') are between 0.3–1.5 μm wide, the low-resolution image also shows extended dark domains with a diameters of 8–15 μm. The extended dark domains in the AFM correlate well with the large dark domains in the fluorescence images in Fig. 2c. The smaller dark domains are just visible in the fluorescence images in Fig. 2. The

height trace of Fig. 4a' shows that the LE phase is rather uniform and ~126 nm thicker than the condensed phase; this corresponds to 20 or more layers in close association with the interface. The LE/LC phase borders are decorated with micron sized domains ~60 nm thicker than the liquid expanded phase, which likely corresponds to Curosurf bilayer aggregates that have not yet spread into the film and roughly correspond to the bright spots in the fluorescence images in Fig. 2. These aggregates are not displaced by motions of the AFM tip, suggesting that the aggregates are connected to the interfacial film.

AFM images of ETS-exposed Curosurf at 40 mN/m (Fig. 4b,b') are qualitatively similar, with a continuous bright yellow LE phase with discrete, dark brown LC phase domains. However, as in Fig. 2, there are significantly fewer large LC phase domains after ETS exposure, there are only the smaller LC domains. The LC phase domains after ETS exposure are (Fig. 4b') relatively monodisperse with a range of 0.2–1 μm, consistent with the fluorescence image in Fig. 2d, which show small, resolution limited black spots. As expected from Fig. 2, few extended dark domains are observed in Fig. 4a'. It appears that ETS exposure prevents the coalescence of the LC domains, suggesting that the line tension between the LC and LE phases decreases [76]. A second major difference due to ETS exposure is revealed in the height trace of Fig. 4b' that shows the LE phase is only ~14 nm thicker than

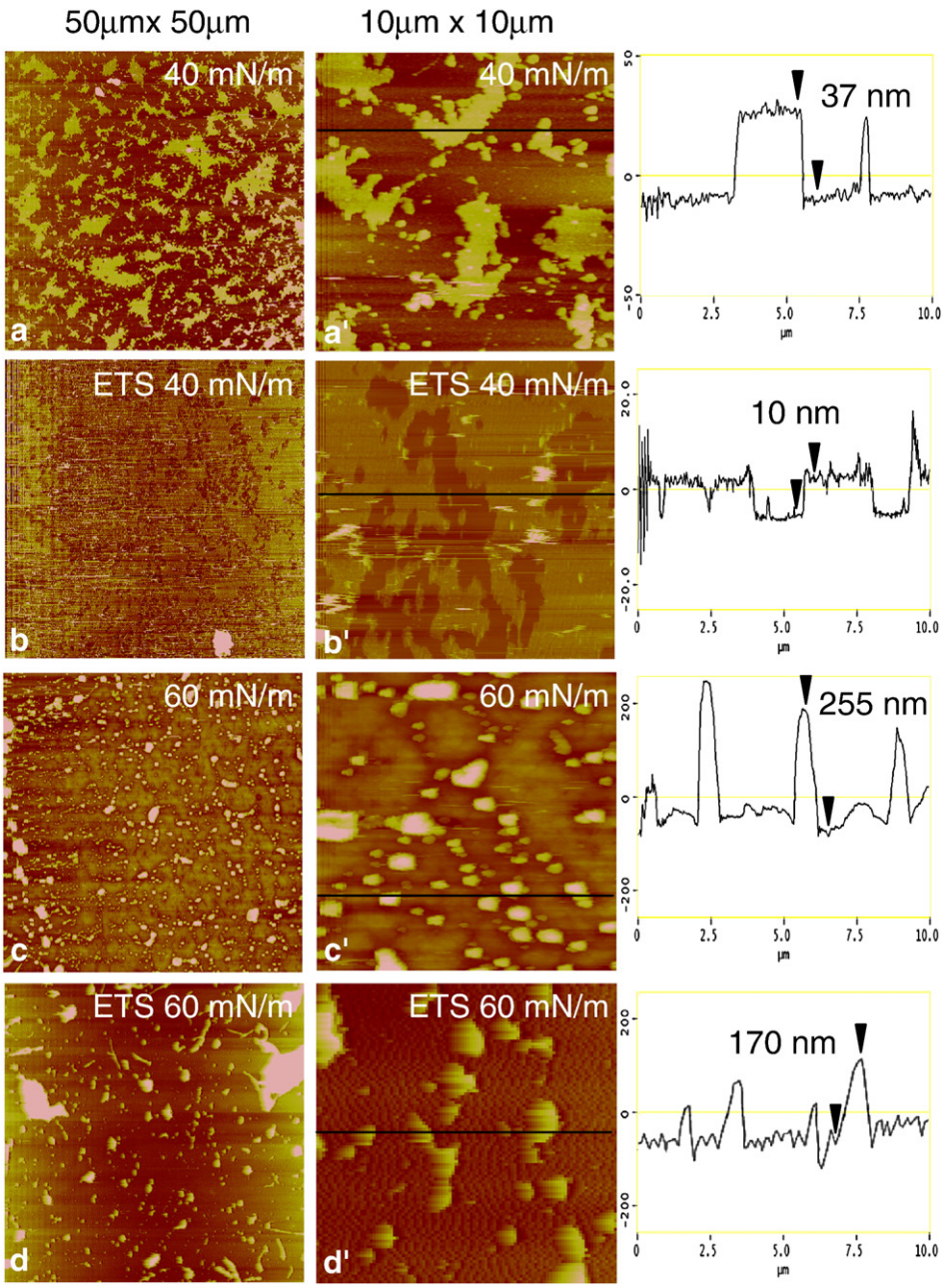

Fig. 5. Atomic force microscopy images of pristine Survanta and ETS-exposed Survanta transferred onto mica substrates by conventional Langmuir–Blodgett deposition. The low resolution images (left column) are 50×50 μm, and the high resolution images (right column) are 10×10 μm sections taken from the low-resolution images. The height trace in the third column corresponds to the black line on each high-resolution image. The brightness in the image increases with the height relative to the mica substrate. Images at 40 mN/m of Survanta at (a) low and (a') high resolution and ETS-exposed Survanta at (b) low and (b') high resolution. While Survanta shows a continuous dark brown network with discrete bright yellow fractal domains, ETS-exposed Survanta shows a greater percentage bright liquid expanded phase. The bright liquid expanded region in Survanta is ~37 nm thicker than the condensed phase versus only ~10 nm thicker in the ETS-exposed Survanta. Images at 60 mN/m of Survanta at (a) low and (a') high resolution and ETS-exposed Survanta at (b) low and (b') high resolution. Both sets of images are dominated by discrete circular raised domains, but the domains are higher and cover a greater area fraction in Survanta indicating that less material is stored near the interface in ETS-exposed Survanta.

the LC phase, with very few bright white spots corresponding to Curosurf aggregates. These images indicate that less surfactant is being stored in the surface associated reservoir near the monolayer in ETS-exposed Curosurf.

Images of Curosurf at 60 mN/m (Fig. 4c,c') show that the LE domains of the film have a patchier, spotted morphology at higher surface pressures. The dark LC domains are more numerous and are ~10 μm wide, similar to their size and appearance at 40 mN/m. These domains also correspond with the condensed phase in the fluorescence images (Fig. 3e) which are ~10 μm in diameter. The smaller LC domains visible in Figs. 4a, a' appear to have coalesced into the larger LC domains. High resolution images (Fig. 4c') show that the formerly continuous liquid expanded film surrounding the dark patches appears to have broken up into small bright, raised domains ~0.3 μm wide and ~116 nm thicker than the dark domains. This may mean that the LE phase lipids are converting into more spheroidal bilayer aggregates that might facilitate transport out of the interfacial reservoir [29].

Images of ETS-exposed Curosurf at 60 mN/m (Fig. 4d,d') also show that the continuous LE phase appears more patchy, with similar spheroidal aggregate structures up to 1.3 μm wide and ~140 nm higher than the background. Fig. 4d' show that there are fewer, but larger diameter bright spots in the ETS-exposed Curosurf compared to the pristine Curosurf (Fig. 4c') and the coverage is not as uniform. In contrast to pristine Curosurf (Fig. 4c), there are no large LC domains in the ETS-exposed Curosurf, consistent with the fluorescence images (Fig. 2f). ETS exposure (Fig. 4d') apparently eliminates the coalescence of the LC domains as well as altering the ways that material is removed from the interface. This alteration of the surface associated reservoir due to ETS-exposure may reduce re-adsorption, leading to less material at the interface, and the changes in the isotherms on repeated cycling as seen in Fig. 1a–b.

At the 40 mN/m, images of Survanta (Fig. 5a) show a continuous dark network with discrete bright, irregularly shaped domains 4–12 μm wide, similar to the morphology of the fluorescence image in Fig. 3c. In contrast to Curosurf (Fig. 4a), the LC phase is the continuous phase in Survanta, and constitutes a larger area fraction than the thicker LE phase, as expected from the greater fraction of saturated lipids in Survanta [16]. The height trace of Fig. 5a' shows that the LE phase domains are ~37 nm thicker than the LC phase regions. In both Survanta and Curosurf, LE phase forms the surface associated reservoir, which is trapped beneath the monolayer during LB deposition. ETS-exposed Survanta (Fig. 5b,b') shows the opposite contrast with interconnected dark domains coexisting within bright interconnected network at 40 mN/m. The bright LE regions make up a greater fraction of the image (Fig. 5b') compared to the pristine Survanta (Fig. 5a'). This is consistent with the fluorescence images of ETS-exposed Survanta (Fig. 3d). However, the height trace of Fig. 5b' reveals that the LE phase is only ~10 nm thicker than the LC phase, which is significantly less than pristine Survanta (Fig. 5a') and may explain why there is a greater fractional coverage of the LE phase in the images. Similar to Curosurf, ETS exposure reduces the amount of material that is being stored in the surface associated reservoir and this appears to alter the distribution of both LC and LE phases at the interface.

At 60 mN/m, Survanta (Fig. 5c,c') appears much more like Curosurf at 60 mN/m (Fig. 4c,c') in that much of the image is are dominated by small spheroidal domains 0.25–1 μm wide and 200–300 nm high on a relatively smooth background (See height trace of Fig. 5c'). The entire underlying film is likely LC phase, similar to the fluorescence images in Fig. 3e. Similar to the Curosurf film (Fig. 4c,c'), the raised domains are likely bilayer aggregates of predominantly unsaturated lipids that have been removed from the interface and stabilized by SP-B and/or SP-C. In contrast to Curosurf (Fig. 4c), the raised domains in Survanta (Fig. 5c) are distributed uniformly throughout the AFM image. The Curosurf film (Fig. 4c,c') retains a much higher density of these raised domains (at high surface pressures) than does the Survanta film, likely due to the higher fraction of SP-B. ETS-exposed Survanta at 60 mN/m (Fig. 5d,d') shows similar raised domains that are larger, more irregularly shaped and less plentiful than pristine Survanta (Fig. 5c, c'). The height trace of Fig. 5d' shows regions 0.5–2 μm wide and 150–200 nm high. The combination of a lower area fraction of raised domains and thinner domains indicates that less material is stored near the interface in the ETS-exposed Survanta (Fig. 5d,d'). Similar to Curosurf, ETS exposure alters the way material is removed from the interface.

4.4. Conformational and chemical analysis of SP-B and SP-C from ETS-exposed surfactants

The morphological changes of Survanta and Curosurf films on ETS-exposure are qualitatively similar, suggesting a decreased function of the lung surfactant specific proteins SP-B and SP-C. Comparison of SP-B protein isolated from ETS-exposed Survanta with that from pristine Survanta samples indicates changes in the secondary structure of the protein as seen by Fourier Transform Infrared (FTIR) spectroscopy (Fig. 6A). In ETS-exposed Survanta, there was a decrease in absorbance centered around 1656 cm^{-1} that is associated with the loss of alpha helical conformations, with enhanced absorbance centered near 1643 and 1630 cm^{-1}, typical of disordered and beta sheet structures. Both of these changes are consistent with oxidation of the SP-B.

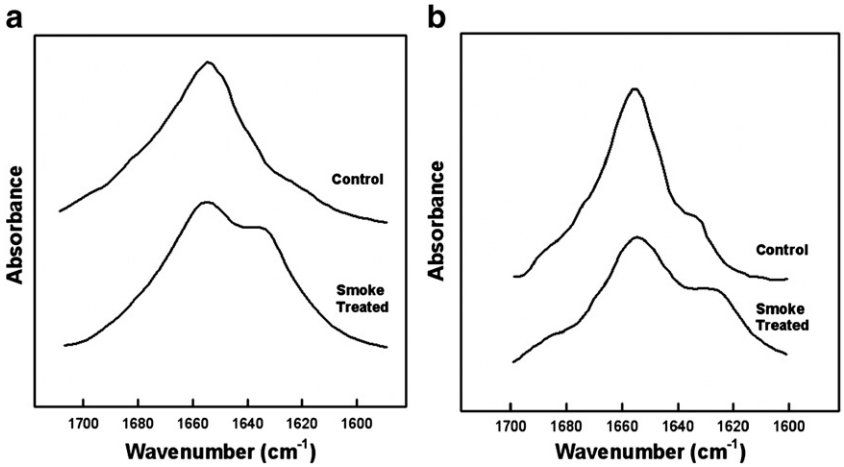

Fig. 6. Stack plots of FTIR spectra of the amide I spectral region of the control and Smoke treated SP-B (a) and SP-C (b). Proteins (100 μg protein) were spread as a self-film in hexafluoroisopropanol (HFIP) and allowed to air dry. The film was then overlaid with HFIP solvent and spectra accumulated and processed as described in the text.

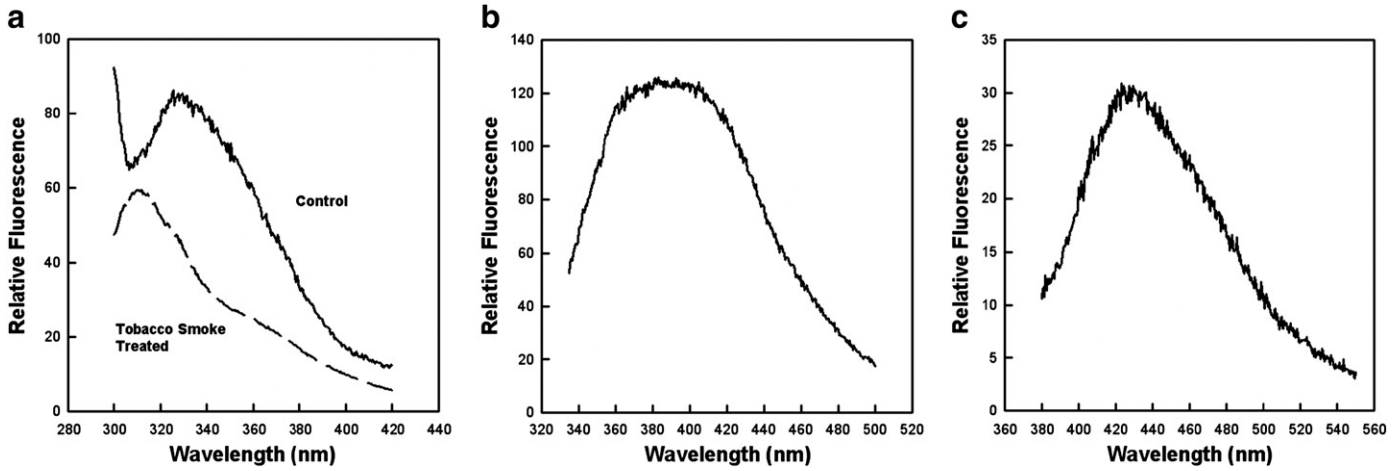

Fig. 7. Fluorescence emission spectra of Trp–Tyr SP-B (50 μg protein/mL) (a) and Fluorescence emission spectra of NFKyn (50 μg protein/mL)(b) and Kyn (50 μg protein/mL) (c) aromatic degradation products associated with smoke treated samples. The control emission spectra were digitally subtracted from the ETS treated sample spectra to obtain the fluorescence emission spectrum of NFKyn and Kyn in the isolated protein sample. Excitation wavelength was at 275 nm for Trp and Tyr, 325 nm for NKFyn and 365 nm for Kyn.

Fluorescence spectroscopy of SP-B extracted from ETS-exposed Survanta indicated the degradation of both tryptophan (Trp) and tyrosine (Tyr) residues. There was a notable loss in fluorescence emission centered around 340 nm attributed to the Trp and Tyr residues in SP-B for ETS-exposed surfactant compared with control protein samples (Fig. 7a). Further fluorescence spectroscopy of the treated samples for aromatic amino acid oxidation revealed the spectral signatures for the tryptophan degradation products *N*-formylkynurenine (NFKyn) (Fig. 7b) and kynurenine (Kyn) (Fig. 7c) consistent with changes in SP-B induced by oxidative chemical treatment of SP-B by Fenton's reagent [38].

Mass spectral analysis of the dimeric bovine SP-B isolated from ETS-exposed Survanta show elevated mass values compared with SP-B from unexposed Survanta, which correlates with the oxidation of tryptophan (Trp) and tyrosine (Tyr) residues observed in the fluorescence measurements. ETS-exposed SP-B had an intense mass peak at 17,562.14 Da with a minor peak at 17,658.43 Da (Fig. 8) compared with a control sample mass of 17,397.7 Da that is close to the calculated mass of dimeric SP-B [36] (not shown). Although the residue-specific modifications cannot be determined from the change in mass alone, such a large alteration of mass seen in ETS-exposed samples is consistent with the oxidation of all four methionines, dihydroxytryptophan, and the formation of NFKyn similar to that observed for other oxidative treatments of SP-B in different lipid monolayers [38].

SP-C also showed spectral changes indicative of changes in the secondary conformation in ETS-exposed Survanta compared with the unexposed protein (Fig. 6b). There was a loss of absorbance centered around 1656 cm^{-1} and enhanced intensity in the range from 1645 to 1620 cm^{-1}, which is typical of a transformation from the dominant alpha helical structure of native SP-C to random to the anti-parallel beta sheet conformations associated with deacylated SP-C [42,43,56]. The loss of thioester linked palmitate residues from SP-C in ETS-exposed Survanta was confirmed by MALDI-TOF spectroscopy. Bovine SP-C isolated from ETS-treated Survanta had an intense signal at 3586.97 Da (Fig. 9) indicative of completely deacylated SP-C [67]. There was also a much less intense peak at 4058.73, indicating that only a minor population of SP-C remained fully acylated.

5. Discussion

Isotherms, FM and AFM images indicate significant changes in the mechanical properties, film morphology and surface associated reservoir [52] upon surfactant exposure to ETS-conditioned water.

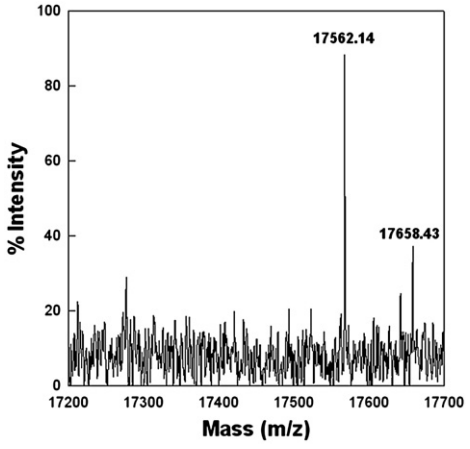

Fig. 8. MALDI-TOF spectrum of Bovine SP-B dimer sample eluted from SDS gel of ETS-exposed surfactant sample. The ABI Voyager-DE STR MALDI-TOF was run in linear mode with delayed extraction and negative polarity. The instrument had an accelerating voltage of 2000 V, an extraction delay time of 125 ns, and a laser intensity of 1925. Treated samples had an intense mass peak at 17,562.14 Da with a minor peak at 17,658.43 Da (this figure) compared with a control sample mass of 17,397.7 Da (not shown) that is close to the calculated mass of dimeric SP-B [36].

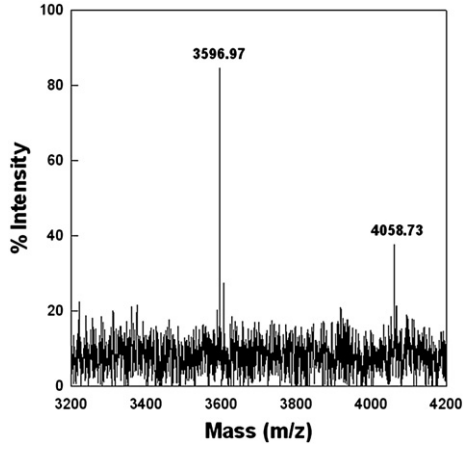

Fig. 9. Maldi-TOF spectrum of isolated Bovine SP-C sample eluted from SDS gel of ETS-treated sample. SP-C isolated from the ETS-treated surfactant had an intense signal at 3586.97 Da indicative of completely deacylated SP-C [42]. There was also a much less intense peak at 4058.73, indicating the presence of a minor population of fully acylated SP-C.

The changes in the isotherms on progressive cycling of the film likely correspond with the observed changes in the interfacial composition. Under normal conditions, the fraction of fluid phase domains, that contain the majority of the unsaturated lipids in the monolayer, decreases with cycling, resulting in an increase in the fraction of solid phase domains, which contain the majority of the saturated lipids [21,29,32,52,54,55,77]. This leads to a stable film that is resistant to collapse [12,18,21,23,25,29,32,33,54,55,63,72]. Unsaturated lipids are not capable of maintaining the high surface pressures (low surface tensions) necessary for proper lung function under normal respiration rates [18,78], so they eventually desorb or are "squeezed-out", likely to the reservoirs of surfactant in the multilayer patches seen in AFM images [21–24,29,32,33,54,55,57]. The multilayer patches may facilitate rapid exchange of reservoir material with subphase material upon expansion and compression or assist with surfactant adsorption from the subphase. As these raised domains are predominantly associated with the liquid expanded phase, it is likely that they are enriched in unsaturated lipids, and the lung surfactant proteins SP-B and SP-C. This may be how the interfacial zone accumulates saturated lipids; the materials that are squeezed out come from the liquid expanded zones of the film and are enriched in unsaturated lipids, while new interface retains the new saturated lipids adsorbing from the subphase. SP-C promotes the formation of multilayer domains [21,24,32,57] and SP-B also forms 3-dimensional structures in the LE phase of simple lipid model mixtures containing unsaturated anionic lipids such as POPG [23]. As the monolayer becomes enriched in saturated lipids, the film becomes more solid-like and elastic and can withstand higher surface pressures before collapsing [29,63,72]. ETS exposure apparently inhibits this process of adsorption and desorption that results in an interfacial refining of the Curosurf film with cycling, preventing the formation of a significant collapse plateau.

The changes we observe depend on the surfactant composition and are more pronounced in Curosurf compared to Survanta. Curosurf contains a greater fraction of unsaturated lipids, 30–40 wt.% wt. vs. 10–25 wt.% for Survanta, as well as higher levels of the surfactant specific protein, SP-B (0.3% (g/g lipid) vs. 0.04–0.13 (g/g lipid)) [16,17]. As a result, Curosurf would require a proportionally greater refinement of the film composition than Survanta (compare Fig. 1a with c) so as to remove sufficient fluid phase (and hence, unsaturated lipids) so that the film can maintain a high surface pressure (low surface tension). Previous work has shown that a minimum LC phase fraction of ~70% correlates with a high surface pressure at film collapse [72]. This minimum LC fraction also leads to a divergence of the surface viscosity for both simple lipid/protein mixtures [36] and for Curosurf and Survanta [22,33]. This increase in the solid phase fraction alters the mechanical properties of the film, resulting in a collapse-resistant film, even under the slow compression rates in the Langmuir trough [63,71]. It is likely that Curosurf cannot reach this minimum level of LC phase after the inhibition of surface refinement by ETS exposure.

While it may be possible for a rapidly compressed monolayer of unsaturated, fluid phase lipid to resist collapse [18,78], a minimum fraction of solid phase appears to be necessary to generate the elastic [54,55,63,71] and viscous [22,33,36] properties of the monolayer to have a high collapse pressure for a wide variety of compression rates. ETS exposure degrades both SP-B and SP-C in Survanta, confirming that these proteins are crucial components to this process. Both SP-B and SP-C are believed to be involved in the transfer of lipid from the monolayer to the surface associated reservoir [12,14,31–33,52,57], and in the adsorption of surfactant from the subphase. Survanta, having a much larger saturated lipid fraction and lower protein levels, likely is always able to reach the minimum LC area fraction for low surface tensions [72], even if the surface refinement is inhibited by ETS exposure. Hence, changes in the Survanta surface associated reservoir have less impact on the mechanical properties of the film compared to Curosurf films.

Fluorescence microscopy and AFM images confirm that the morphology of Curosurf changes more on ETS exposure than Survanta. In Curosurf, fluorescence microscopy images show that ETS exposure inhibits the coalescence of small, 0.5–2 μm diameter LC domains, thereby limiting the formation of larger, 8–20 μm diameter LC domains (8–12 μm). This suggests that ETS contains or induces the formation of chemical species capable of lowering the line tension between the condensed and liquid expanded domains thereby minimizing LC domain growth [62,76,79]. AFM images show that both Curosurf and Survanta, when adsorbed from the subphase, form complex, multilayer films [33] that are structurally quite different than lipid or lipid/protein films spread from solvent [21,24,32,74]. There is a good correspondence between the morphology and distribution of the LE and LC phase domains as imaged by AFM and FM, suggesting that there is minimal rearrangement of the films during Langmuir–Blodgett deposition. The images at 40 mN/m demonstrate that ETS exposure reduces the amount of material in the surface associated reservoir; the thickness of the liquid expanded phase is reduced from ~126 nm to ~14 nm in Curosurf and from ~37 nm to ~10 nm in Survanta. At 60 mN/m, the Curosurf and Survanta images reveal that the liquid expanded phase is heterogeneous and consists of discrete spheroidal aggregates likely enriched in unsaturated lipids stabilized by SP-B and SP-C. In both Curosurf and Survanta, ETS exposure results in fewer aggregates, indicating that less material is stored near the interface after ETS exposure.

The AFM images confirm that ETS reduces the amount of material in the surface associated reservoir and alters the way material is adsorbed and desorbed from the interface. While the effect on the surface associated reservoir is similar for both surfactants, the impact on maximum surface pressure is greater for Curosurf than Survanta due to the greater refinement required by the Curosurf film to sustain high surface pressures. Our results are consistent with previous work using model lipid mixtures where ETS exposure resulted in poor respreading after collapse, a loss of surfactant material on cycling and lower maximum surface pressures [37]. However, for the pure lipid systems, we did not observe any multilayer reservoir formation in either pristine or ETS-exposed lipids, which suggests that the reservoir is due to adsorption and desorption from the subphase.

The stability and extent of the multilayer reservoir is likely related to the presence of SP-B and SP-C. Oxidation of the Trp and Tyr amino acids, along with the changes in secondary structure on ETS exposure of SP-B in Survanta suggests that a corresponding degradation in the function of SP-B may be partially responsible for the morphological changes we see in the films [22,23,32,33,52,53]. Similar changes in the hydrophobic amino acid side chains of SP-B have also been observed due to oxidation in Fenton reagent-treated surfactant extracts of different lipid composition than either Survanta or Curosurf [38]. These changes in the hydrophobic protein side chain chemistry correlated with a decrease in phospholipid respreading during the compression and expansion of the surfactant film as well as the failure of these films to attain low surface tensions during compression as we observe here.

Similarly the chemical alteration of the SP-C protein in Survanta by deacylation has been shown to decrease the surface activity of surfactant dispersions and enhance beta-sheet conformations at the expense of the dominant alpha-helix [42,43,56], correlating the changes in the chemical composition and secondary structure of the amphipathic surfactant protein with altered morphology and function. SP-C helps stabilize multilayer formation due to its hydrophobic helical structure which can insert normal to the bilayer; the fatty acid chains on SP-C can anchor one bilayer to another, greatly increasing the stability of the surface-associated reservoir [21,22,32,33,57]. SP-C primarily alters the distribution of unsaturated lipids, Flach et al. [80] showed minimal alterations in pure DPPC films on deacylation, while Wang et al. [43] showed significant changes in isotherms and adsorption of mixed saturated and unsaturated lipids similar to

those reported here. As SP-C appears to primarily affect the LE phase that contains the unsaturated lipids, it is not surprising that films with no unsaturated lipids would be relatively unaltered, similar to Survanta, while films with more unsaturated lipids, similar to Curosurf, would be altered more significantly, as we observe. Deacylation and loss of helical secondary structure of SP-C may be why we see such a noticeable decrease in the amount of material trapped in the surface associated reservoir in the Curosurf films; there is simply less functional SP-C to mechanically reinforce the multilayers [57].

While the impact of ETS exposure on lung surfactant lipid and protein chemistry and morphology was assessed in this study, there are additional effects of ETS exposure that can further compromise lung surfactant function. Only those components of ETS that are water-soluble can interact with the surfactant in our model system; hence, we are probably underestimating the actual effects of ETS on surfactant. While direct exposure of the surfactant interfacial film to tobacco smoke is also possible, it would lead to artifacts that would confuse interpretation of the AFM and FM images, obscuring the physical and chemical interactions between the lung surfactant and water soluble compounds in ETS. Several isotherm measurements by Subramaniam et. al have shown that exposure to tobacco smoke (mainstream or ETS) affects the mechanical properties of lung surfactant in agreement with our current findings using ETS-exposed surfactants [48,49].

6. Conclusions

ETS exposure modifies the chemical, mechanical and morphological properties at the air–liquid interface of the clinical replacement lung surfactants Curosurf and Survanta, thereby reducing their effectiveness at lowering surface tension *in vitro*. AFM images of Survanta and Curosurf show that ETS reduces the amount of material near the interface and alters how surfactant is adsorbed and desorbed from the interface during compression/expansion cycles. In Curosurf, the films cannot be sufficiently refined to reach the minimum level of LC phase [72], which leads to higher minimum surface tensions. These effects are likely due to the oxidation of the surfactant specific protein SP-B and deacylation of SP-C we observe in Survanta films, which inhibits the proteins' ability to promote exchange between the surface-associated reservoir [52] and the active monolayer [21,23,29,32,43]. ETS also changes the lateral distribution of LE and LC domains in the Curosurf film, reducing the line tension between the liquid expanded and condensed phases [79]. This prevents the coalescence of small LC domains to larger ones that may lead to lower surface tensions [72]. In contrast, the minimum surface tension of the Survanta film is less impacted by ETS exposure as expected from its smaller fraction of unsaturated lipids and surfactant proteins. Exposure to ETS increases the work of breathing by destabilizing the surfactant associated reservoir and refining of the interfacial film, both of which lead to higher minimum surface tension during the breathing cycle.

Acknowledgments

We thank Bill Taeusch for ongoing collaborations on surfactant adsorption and Dale Uyeminami for preparing the smoke-conditioned water. Support for this work comes from National Institute of Health Grants HL-66410 (AJW), HL-51177 (JAZ), and ES011634 (KEP) and the Tobacco Related Disease Research Program 14RT-0077 (JAZ, AJW) and 7RT-0118 (KEP). P.C.S. was partially supported by a NSF graduate research fellowship.

References

[1] M. Chan-Yeung, H. Dimich-Ward, Respiratory health effects of exposure to environmental tobacco smoke, Respirology 8 (2003) 131–139.
[2] S.V. Teague, K.E. Pinkerton, M. Goldsmith, A. Gebremichael, S. Chang, R.A. Jenkins, J.H. Moneyhun, Sidestream cigarette-smoke generation and exposure system for environmental tobacco-smoke studies, Inhal. Toxicol. 6 (1994) 79–93.
[3] F. Adlkofer, Lung cancer due to passive smoking — a review, Int. Arch. Occup. Environ. Health 74 (2001) 231–241.
[4] A. Dunn, L. Zeine, California Environmental Protection Agency, Sacramento, CA, 1997.
[5] C. Janson, The effect of passive smoking on respiratory health in children and adults, Int. J. Tuberc. Lung Dis. 8 (2004) 510–516.
[6] K.C. Johnson, J.F. Hu, Y. Mao, Lifetime residential and workplace exposure to environmental tobacco smoke and lung cancer in never-smoking women, Canada 1994–97, Int. J. Cancer 93 (2001) 902–906.
[7] M.L. Larsson, M. Frisk, J. Hallstrom, J. Kiviloog, B. Lundback, Environmental tobacco smoke exposure during childhood is associated with increased prevalence of asthma in adults, Chest 120 (2001) 711–717.
[8] F.D. Gilliland, Y.F. Li, J.M. Peters, Effects of maternal smoking during pregnancy and environmental tobacco smoke on asthma and wheezing in children, Am. J. Respir. Crit. Care Med. 163 (2001) 429–436.
[9] E. Putman, L.M.G. vanGolde, H.P. Haagsman, Toxic oxidant species and their impact on the pulmonary surfactant system, Lung 175 (1997) 75–103.
[10] J.A. Clements, M.E. Avery, Lung surfactant and neonatal respiratory distress syndrome, Am. J. Respir. Crit. Care Med. 157 (1998) S59–S66.
[11] M.E. Avery, Surfactant deficiency in hyaline membrane disease — the story of discovery, Am. J. Respir. Crit. Care Med. 161 (2000) 1074–1075.
[12] R. Notter, Lung Surfactant: Basic Science and Clinical Applications, Marcel Dekker, New York, 2000.
[13] J.A. Zasadzinski, J. Ding, H.E. Warriner, F. Bringezu, A.J. Waring, The physics and physiology of lung surfactants, Curr. Opin. Colloid Interface Sci. 6 (2001) 506–513.
[14] J. Perez-Gil, Structure of pulmonary surfactant membranes and films: the role of proteins and lipid–protein interactions, Biochim. Biophys. Acta, (BBA)-Biomembr. 1778 (2008) 1676–1695.
[15] Y.Y. Zuo, R.A. Veldhuizen, A.W. Neumann, N.O. Peterson, F. Possmayer, Current perspectives in pulmonary surfactant — inhibition, enhancement and evaluation, Biochim. Biophys. Acta 1778 (2008) 1947–1977.
[16] W. Bernhard, J. Mottaghian, A. Gebert, G.A. Rau, H. von der Hardt, C.F. Poets, Commercial versus native surfactants — surface activity, molecular components, and the effect of calcium, Am. J. Respir. Crit. Care Med. 162 (2000) 1524–1533.
[17] A. Braun, P.C. Stenger, H.E. Warriner, J.A. Zasadzinski, K.W. Lu, H.W. Taeusch, A freeze-fracture transmission electron microscope and small angle X-ray diffraction study of the effects of albumin, Serum and polymers on clinical lung surfactant microstructure, Biophys. J. 93 (2007) 123–139.
[18] E.C. Smith, J.M. Crane, T.G. Laderas, S.B. Hall, Metastability of a supercompressed fluid monolayer, Biophys. J. 85 (2003) 3048–3057.
[19] F. Lhert, W. Yan, S.C. Biswas, S.B. Hall, Effects of hydrophobic surfactant proteins on collapse of pulmonary surfactant monolayers, Biophys. J. 93 (2007) 4237–4243.
[20] K.Y.C. Lee, J. Majewski, T.L. Kuhl, P.B. Howes, K. Kjaer, M.M. Lipp, A. Waring, J.A. Zasadzinski, G.S. Smith, Synchrotron X-ray study of lung surfactant specific protein SP-B in lipid monolayers, Biophys. J. 81 (2001) 572–585.
[21] J.Q. Ding, D.Y. Takamoto, A. von Nahmen, M.M. Lipp, K.Y.C. Lee, A.J. Waring, J.A. Zasadzinski, Effects of lung surfactant proteins, SP-B and SP-C, and palmitic acid on monolayer stability, Biophys. J. 80 (2001) 2262–2272.
[22] C. Alonso, A. Waring, J.A. Zasadzinski, Keeping lung surfactant where it belongs: protein regulation of two-dimensional viscosity, Biophys. J. 89 (2005) 266–273.
[23] J.Q. Ding, I. Doudevski, H.E. Warriner, T. Alig, J.A. Zasadzinski, Nanostructure changes in lung surfactant monolayers induced by interactions between palmitoyloleoylphosphatidylglycerol and surfactant protein B, Langmuir 19 (2003) 1539–1550.
[24] D.Y. Takamoto, M.M. Lipp, A. von Nahmen, K.Y.C. Lee, A.J. Waring, J.A. Zasadzinski, Interaction of lung surfactant proteins with anionic phospholipids, Biophys. J. 81 (2001) 153–169.
[25] K.Y.C. Lee, A. Gopal, A. von Nahmen, J.A. Zasadzinski, J. Majewski, G.S. Smith, P.B. Howes, K. Kjaer, Influence of palmitic acid and hexadecanol on the phase transition temperature and molecular packing of dipalmitoylphosphatidylcholine monolayers at the air-water interface, J. Chem. Phys. 116 (2002) 774–783.
[26] C. Alonso, F. Bringezu, G. Brezesinski, A.J. Waring, J.A. Zasadzinski, Modifying calf lung surfactant by hexadecanol, Langmuir 21 (2005) 1028–1035.
[27] I. Plasencia, K.M.W. Keough, J. Perez-Gil, Interaction of the N-terminal segment of pulmonary surfactant protein SP-C with interfacial phospholipid films, Biochim. Biophys. Acta 1713 (2005) 118–128.
[28] L. Gunasekara, W.M. Schoel, S. Schürch, M.W. Amrein, A comparative study of mechanisms of surfactant inhibition, Biochim. Biophys. Acta 1778 (2008) 433–444.
[29] M.M. Lipp, K.Y.C. Lee, D.Y. Takamoto, J.A. Zasadzinski, A.J. Waring, Coexistence of buckled and flat monolayers, Phys. Rev. Lett. 81 (1998) 1650–1653.
[30] J. Goerke, Pulmonary surfactant: functions and molecular composition, Biochim. Biophys. Acta, Mol. Basis Dis. 1408 (1998) 79–89.
[31] J. Johansson, Structure and properties of surfactant protein C, Biochim. Biophys. Acta, Mol. Basis Dis. 1408 (1998) 161–172.
[32] A. vonNahmen, M. Schenk, M. Sieber, M. Amrein, The structure of a model pulmonary surfactant as revealed by scanning force microscopy, Biophys. J. 72 (1997) 463–469.
[33] C. Alonso, T. Alig, J. Yoon, F. Bringezu, H. Warriner, J.A. Zasadzinski, More than a monolayer: relating lung surfactant structure and mechanics to composition, Biophys. J. 87 (2004) 4188–4202.

[34] R. Veldhuizen, K. Nag, S. Orgeig, F. Possmayer, The role of lipids in pulmonary surfactant, Biochim. Biophys. Acta, Mol. Basis Dis. 1408 (1998) 90–108.
[35] F. Bringezu, J.Q. Ding, G. Brezesinski, J.A. Zasadzinski, Changes in model lung surfactant monolayers induced by palmitic acid, Langmuir 17 (2001) 4641–4648.
[36] J.Q. Ding, H.E. Warriner, J.A. Zasadzinski, Viscosity of two-dimensional suspensions, Phys. Rev. Lett. 88 (2002) 168102.
[37] F. Bringezu, K.E. Pinkerton, J.A. Zasadzinski, Environmental tobacco smoke effects on the primary lipids of lung surfactant, Langmuir 19 (2003) 2900–2907.
[38] D. Manzanares, K. Rodriguez-Capote, S.C. Liu, T. Haines, Y. Ramos, L. Zhao, A. Doherty-Kirby, G. Lajoie, F. Possmayer, Modification of tryptophan and methionine residues is implicated in the oxidative inactivation of Surfactant Protein B, Biochemistry 46 (2007) 5604–5615.
[39] K. Rodriguez-Capote, D. Manzanares, T. Haines, F. Possmayer, Reactive oxygen species inactivation of surfactant involves structural and functional alterations to surfactant proteins SP-B and SP-C, Biophys. J. 90 (2006) 2808–2821.
[40] O. Blanco, J. Perez-Gil, Biochemical and pharmacological differences between preparations of exogenous natural surfactant used to treat RDS, Eur. J. Pharmacol. 568 (2007) 1–15.
[41] S. Orgeig, C.B. Daniels, The roles of cholesterol in pulmonary surfactant: insights from comparative and evolutionary studies, Comp. Biochem. Phys. A 129 (2001) 75–89.
[42] R.A. Dluhy, S. Shanmukh, J.b. Leapard, P. Kruger, J.E. Baatz, Deacylated pulmonary surfactant protein SP-C transforms from alpha-helical to amyloid fibril structures via a pH dependent mechanism: an infrared structural investigation, Biophys. J. 85 (2003) 2417–2429.
[43] Z. Wang, O. Gurel, J.E. Baatz, R.H. Notter, Acylation of pulmonary surfactant protein-C is required for its optimal surface active interactions with phospholipids, J. Biol. Chem. 271 (1996) 19104–19109.
[44] M.M. Lee, F.H.Y. Green, S. Schurch, S. Cheng, S.G. Bjarnason, S. Leonard, W. Wallace, F. Possmayer, V. Vallyathan, Comparison of inhibitory effects of oxygen radicals and calf serum protein on surfactant activity, Mol. Cell. Biochem. 259 (2004) 15–22.
[45] C.M. Chen, L.F. Wang, T.F. Yeh, Effects of maternal nicotine exposure on lung surfactant system in rats, Pediatr. Pulmonol. 39 (2005) 97–102.
[46] Y. Honda, H. Takahashi, Y. Kuroki, T. Akino, S. Abe, Decreased contents of surfactant proteins A and D in BAL fluids of healthy smokers, Chest 109 (1996) 1006–1009.
[47] M. Robin, P. Dong, C. Hermans, A. Bernard, A.D. Bersten, I.R. Doyle, Serum levels of CC16, SP-A and SP-B reflect tobacco-smoke exclosure in asymptomatic subjects, Eur. Respir. J. 20 (2002) 1152–1161.
[48] S. Subramaniam, P. Bummer, C.G. Gairola, Biochemical and biophysical characterization of pulmonary surfactant in rats exposed chronically to cigarette-smoke, Fundam. Appl. Toxicol. 27 (1995) 63–69.
[49] S. Subramaniam, S. Srinivasan, P.M. Bummer, C.G. Gairola, Perinatal sidestream cigarette smoke exposure and the developing pulmonary surfactant system in rats, Human Exp. Toxicol. 18 (1999) 206–211.
[50] S. Subramaniam, J.A. Whitsett, W. Hull, C.G. Gairola, Alteration of pulmonary surfactant proteins in rats chronically exposed to cigarette smoke, Toxicol. Appl. Pharmacol. 140 (1996) 274–280.
[51] Y. Xue, T.L. Williams, T. Li, J. Umbehr, L. Fang, W.Q. Wang, R.C. Baybutt, Type II pneumocytes modulate surfactant production in response to cigarette smoke constituents: restoration by vitamins A and E, Toxicol. in Vitro 19 (2005) 1061–1069.
[52] S. Schürch, F.H.Y. Green, H. Bachofen, Formation and structure of surface films: captive bubble surfactometry, Biochim. Biophys. Acta 1408 (1998) 180–202.
[53] S. Schürch, R. Qanbar, H. Bachofen, F. Possmayer, The surface-associated surfactant reservoir in the alveolar lining, Biol. Neonate 67 (1995) 61–76.
[54] Y.Y. Zuo, S.M. Takayyon, E. Keaing, L. Zhao, R.A. Veldhuizen, N.O. Peterson, M.W. Amrein, F. Possmayer, Atomic force microscopy studies of functional and dysfunctional pulmonary surfactant films, II. Albumin-inhibited surfactant films and the effects of SP-A, Biophys. J. 95 (2008) 2779–2791.
[55] Y.Y. Zuo, S.M. Takayyon, E. Keaing, L. Zhao, R.A. Veldhuizen, N.O. Peterson, M.W. Amrein, F. Possmayer, Atomic force microscopy studies of functional and dysfunctional pulmonary surfactant films, I. Micro and nanostructures of functional pulmonary surfactant films and the effect of SP-A, Biophys. J. 94 (2008) 3459–3564.
[56] G. Vandenbussche, A. Clercx, T. Curstedt, J. Johannsson, H. Jornvall, J.-M. Ruysschaert, Structure and orientation of the surfactant associated protein C in a lipid bilayer, Eur. J. Biochem. 203 (1992) 201–209.
[57] Z. Leonenko, M. Rodenstein, J. Dohner, L.M. Eng, M.W. Amrein, Electrical surface potential of pulmonary surfactant, Langmuir 21 (2006) 10135–10139.
[58] J. Folch, M. Lees, G.H. Sloane-Stanley, A simple method for the isolation and purification of total lipids from animal tissues, J. Biol. Chem. 226 (1957) 497–505.
[59] J.E. Baatz, Y. Zou, J.T. Cox, Z. Wang, R.H. Notter, High-yield purification of lung surfactant protein SP-B and SP-C and the effects of surface activity, Protein Expr. Purif. 23 (2001) 180–190.
[60] P.C. Stenger, J.A. Zasadzinski, Enhanced surfactant adsorption via polymer depletion forces: a simple model for reversing surfactant inhibition in acute respiratory distress syndrome, Biophys. J. 92 (2007) 3–9.
[61] P.S. Stenger, S.G Isbell and J.A. Zasadzinski, Molecular weight dependence of the depletion attraction and its effects on the competitive adsorption of lung surfactant. Biochim. Biophys. Acta DOI information: 10.1016/j.bbamem.2008.03.019 (2008).
[62] H.M. McConnell, Structures and transitions in lipid monolayers at the air–water-interface, Annu. Rev. Phys. chem. 42 (1991) 171–195.
[63] L. Pocivavsek, R. Dellsy, A. Kern, S. Johnson, B. Lin, K.Y.C. Lee, E. Cerda, Stress and fold localization in thin elastic membranes, Science 320 (2008) 912–916.
[64] J. Garnaes, D.K. Schwartz, R. Viswanathan, J. Zasadzinski, Domain boundaries and buckling superstructures in Langmuir–Blodgett films, Nature 357 (1992) 54–57.
[65] D.Y. Takamoto, E. Aydil, J.A. Zasadzinski, A. Ivanova, D.K. Schwartz, T. Yang, P. Cremer, Stable ordering in Langmuir–Blodgett films, Science 293 (2001) 1292–1295.
[66] L.M. Gordon, K.Y.C. Lee, J.A. Zasadzinski, F.J. Walther, M.A. Sherman, A.J. Waring, Conformational mapping of the N-terminal segment of surfactant protein B in lipid using 13C-enhanced Fourier transform infrared spectroscopy, J. Peptide Res. 55 (2000) 330–347.
[67] L.M. Gordon, P.W. Mobley, R. Pilpa, M.A. Sherman, A.J. Waring, Conformational mapping of the N-terminal peptide of HIV-1 gp41 in membrane environments using 13C-enhanced Fourier transform infrared spectroscopy, Biochim. Biophys. Acta 1559 (2002) 96–120.
[68] D.M. Byler, H. Susi, Examination of the secondary structure of proteins by deconvoluted FTIR, Biopolymers 25 (1986) 465–487.
[69] J.A. Clements, Surface tension of lung extracts, Proc. Soc. Exp. Biol. Med. 95 (1957) 170–172.
[70] H.W. Taeusch, J.B. de la Serna, J. Perez-Gil, C. Alonso, J.A. Zasadzinski, Inactivation of pulmonary surfactant due to serum-inhibited adsorption and reversal by hydrophilic polymers: Experimental, Biophys. J. 89 (2005) 1769–1779.
[71] W. Lu, C.M. Knobler, R.F. Bruinsma, M. Twardos, M. Dennin, Folding Langmuir monolayers, Phys. Rev. Lett. 89 (2002) 146107.
[72] A. Gopal, K.Y.C. Lee, Headgroup percolation and collapse of condensed Langmuir monolayers, J. Phys. Chem. B 110 (2006) 22079–22087.
[73] J.A. Zasadzinski, R. Viswanathan, L. Madsen, J. Garnaes, D.K. Schwartz, Langmuir–Blodgett Films, Science 263 (1994) 1726–1733.
[74] A. Cruz, L. Vazquez, M. Velez, J. Perez-Gil, Effect of pulmonary surfactant protein SP-B on the micro- and nanostructure of phospholipid films, Biophys. J. 86 (2004) 308–320.
[75] K. Winsel, D. Honig, K. Lunkenheimer, K. Geggel, C. Witt, Quantitative Brewster angle microscopy of the surface film of human broncho-alveolar lavage fluid, Eur. Biophys. J. Biophys. Lett. 32 (2003) 544–552.
[76] M. Seul, D. Andelman, Domain shapes and patterns: the phenomenology of modulated phases, Science 267 (1995) 476–483.
[77] K. Nag, J. Perez-Gil, M.L. Ruano, L.A. Worthman, J. Stewart, C. Casals, K.M.W. Keough, Phase transitions in films of lung surfactant at the air–water interface, Biophys. J. 74 (1998) 2983–2995.
[78] W. Yan, S.C. Biswas, T.G. Laderas, S.B. Hall, The melting of pulmonary surfactant monolayers, J. Appl. Physiol. 102 (2007) 1739–1745.
[79] S.L. Keller, W.H.I. Pitcher, W.H. Huestis, H.M. McConnell, Red blood cell lipids form immisible liquids, Phys. Rev. Lett. 81 (1998) 5019–5022.
[80] C.R. Flach, A. Gericke, K.M. Keough, R. Mendelsohn, Palmitoylation of lung surfactant protein SP-C alters surface thermodynamics, but not protein secondary structure or orientation in DPPC films, Biochim. Biophys. Acta 1416 (1999) 11–20.